

Effect of social group dynamics on contagionZhenyuan Zhao,¹ J. P. Calderón,² Chen Xu,³ Guannan Zhao,¹ Dan Fenn,⁴ Didier Sornette,⁵ Riley Crane,⁵ Pak Ming Hui,⁶ and Neil F. Johnson¹¹*Physics Department, University of Miami, Coral Gables, Florida 33126, USA*²*Industrial Engineering Department, Universidad de Los Andes, Bogota, Colombia*³*School of Physical Science and Technology, Soochow University, Suzhou 215006, People's Republic of China*⁴*Oxford Centre for Industrial and Applied Maths, Oxford University, Oxford OX1 3PU, United Kingdom*⁵*ETH Zurich, D-MTEC, Kreuzplatz 5, 8001 Zurich, Switzerland*⁶*Department of Physics, The Chinese University of Hong Kong, Shatin, Hong Kong*

(Received 16 October 2009; revised manuscript received 19 March 2010; published 25 May 2010)

Despite the many works on contagion phenomena in both well-mixed systems and heterogeneous networks, there is still a lack of understanding of the intermediate regime where social group structures evolve on a similar time scale to individual-level transmission. We address this question by considering the process of transmission through a model population comprising social groups which follow simple dynamical rules for growth and breakup. Despite the simplicity of our model, the profiles produced bear a striking resemblance to a wide variety of real-world examples—in particular, empirical data that we have obtained for social (i.e., YouTube), financial (i.e., currency markets), and biological (i.e., colds in schools) systems. The observation of multiple resurgent peaks and abnormal decay times is qualitatively reproduced within the model simply by varying the time scales for group coalescence and fragmentation. We provide an approximate analytic treatment of the system and highlight a novel transition which arises as a result of the social group dynamics.

DOI: [10.1103/PhysRevE.81.056107](https://doi.org/10.1103/PhysRevE.81.056107)

PACS number(s): 89.75.Hc, 87.23.Ge, 87.23.Cc, 87.18.-h

I. INTRODUCTION

The world recently witnessed a baffling variety of global outbreak phenomena: the huge fluctuations across the world's financial markets, driven in part by the rapid global spread of rumors [1]; an unexpected global outbreak of swine flu [2], driven in part by rapid social mixing (e.g., within schools [3]); and even the sudden rise to global fame of an unknown Scottish singer, driven in part by word-of-mouth sharing [4–6]. To understand how such phenomena might arise, consider the following: The number and identity of the people with whom we are each in instantaneous electronic or physical contact—and with whom we can therefore instantaneously exchange information, rumors or viruses—can change slowly or rapidly within any given day, according to the activities which we undertake and hence the instantaneous social groups within which we happen to find ourselves. Even on the shortest plane journeys, for example, passengers find themselves momentarily confined in an enclosed space with complete strangers for up to an hour or more, enabling the exchange of respiratory pathogens. On the blogosphere and on the web, ephemeral groups form around topics or content and exchange information, opinions, and social contacts before flickering out of existence. The transient transnational nature of online discussion groups and chat rooms, as frequented by financial traders or YouTube users [1,5,6] provides a vivid illustration. A full description of such specific transmission processes would likely require rather sophisticated epidemiological models which incorporate system-specific details and considerations (e.g., spatial topology, differential susceptibility). There are indeed many sophisticated epidemiological models already under construction and study in the literature [7–16]. Some of these focus on the well-mixed (i.e., mass-action) limit, some of

these focus on the limit of heterogeneous networks [10,13–16]—and some attempt to move between the two by adding patchlike structure to mass-action models or dynamical link rewirings to network models.

In this paper, we focus on the less well understood dynamical regime where the group-level dynamics and individual-level transmission processes can evolve on the same time scale, and hence the number and identity of a given individual's contacts can change abruptly at any given moment in time [see, for example, Figs. 1(a) and 1(b)]. In Sec. II, we introduce and analyze a simple model which mimics the dynamical processes of social group formation or breakup and person-to-person transmission of a virus or information, allowing them to coexist on comparable time scales. By varying the probabilities of group coalescence (ν_{coal}) and fragmentation (ν_{frag}) relative to the standard SIR (susceptible \rightarrow infected \rightarrow recovered) probabilities [7,12] for person-to-person transmission (p) and individual recovery (q), the entire range of relative time scales can be easily explored—from a very slowly changing social network structure (i.e., essentially a static network with infrequent rewirings) through to a rapidly changing social network structure (i.e., essentially a well-mixed population). Most importantly, this includes the complicated intermediate regime where both processes coexist on the same time scale. Figure 1 illustrates this intermediate regime, while Fig. 2 shows how an associated infection profile $I(t)$ is qualitatively very different from the two limiting cases of the static (or quasi-static) network, and the well-mixed population. Instead, the interplay of the group dynamics and individual-level transmission generates epidemic profiles which exhibit a rich structure (e.g., multiple resurgences and abnormal decay times, see Fig. 2). It turns out that such profiles are strikingly similar to real-world outbreaks across the social, financial, and biological domains (see Fig. 3 and Sec. III). While it is

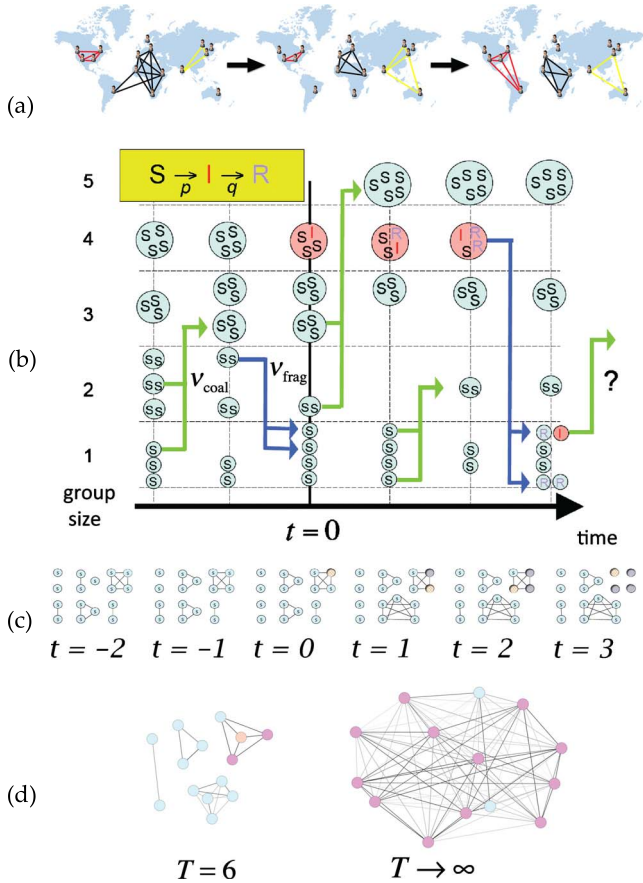


FIG. 1. (Color online) (a) Schematic of dynamical grouping of traders or YouTube users on the Internet. (b) Schematic of our model, featuring spreading in the presence of dynamical grouping via coalescence and fragmentation. Vertical axis shows number of groups of a given size at time t . (c) Instantaneous network from Fig. 1(b) at each time step. (d) Weighted network obtained by aggregating links over time-window T .

conceivable that infection profiles similar to Fig. 3 can also be obtained using alternative, more sophisticated epidemiological models (e.g., by adding spatial topology or differential susceptibility), such models will typically have more parameters and be more system specific. By contrast, our model only has four stochastic parameters for the probabilities (and hence time scales) of the individual-level transmission and group dynamics, i.e., p, q for the SIR process, and ν_{coal} and ν_{frag} which describe the probability of social groups coalescing or fragmenting. We find it intriguing that the qualitative shapes of such a wide range of empirical profiles (Fig. 3) can be reproduced simply by varying these relative time scales. While we cannot prove that the empirically observed profiles in Fig. 3 are indeed generated by such a simple model as ours, it seems that more complex models are not required in order to reproduce their main features. In Sec. IV, we offer an approximate analytic analysis of the properties of our model. Although a detailed theoretical description of the infection profiles $I(t)$ remains an open future challenge, we find that the overall properties can be captured by making a mean-field approximation of the behavior of

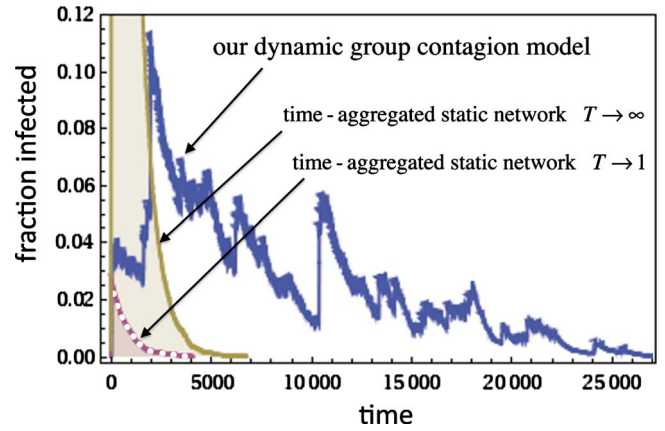


FIG. 2. (Color online) Theoretical profile $I(t)$. Thick (blue) curve shows our dynamical group contagion model, with $\nu_{frag} = 0.05$, $\nu_{coal} = 0.95$, $p = 0.001$, and $q = 0.001$. Using same p and q values, dotted (purple) curve corresponds to stochastic SIR model on a static network with $T \rightarrow 1$, i.e., the $t = 0$ network in Fig. 1. Thin solid (green) curve corresponds to stochastic SIR on a $T \rightarrow \infty$ network.

connected pairs within the population. In Sec. V, we comment on how our results also suggest a minimally invasive dynamical method for controlling outbreaks (see Fig. 5). Section VI extends the discussion to other types of viral

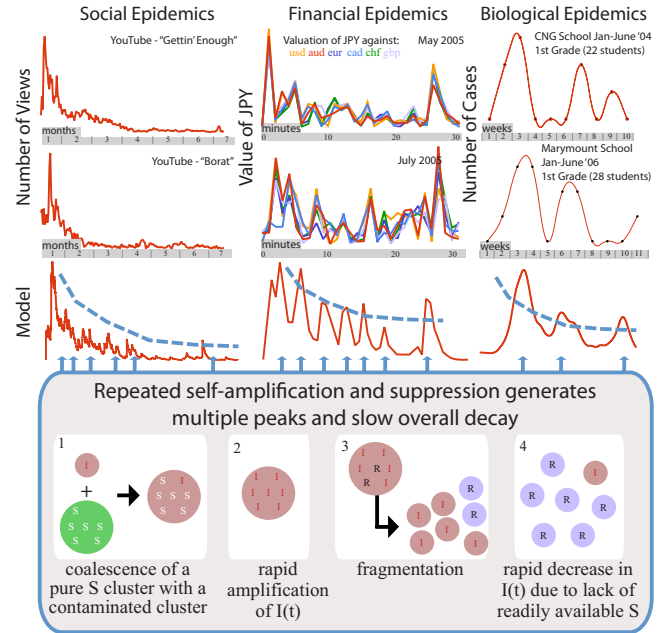


FIG. 3. (Color online) Top two rows: empirical activity profile $I(t)$ in three distinct real-world systems. Third row: results from our model. Dashed line is a guide to the eyes. Left: YouTube download activity. Middle: currency trading activity (i.e., absolute value of price-change, hence the excess demand to buy or sell at each time step). Different shades correspond to different currencies. See main text. Right: fraction of children with colds within a school. Lower panel: simple example of the repeated self-amplification and suppression processes which spontaneously arise within our model. When replicated at all scales of group size, these processes generate a unified quantitative description of the empirical $I(t)$ profiles.

transmission models which are widely studied in the literature (e.g., SIS). Section VII provides a summary and outlook.

II. OUR MODEL

There are many plausible rules for generating human group dynamics [17]. The grouping process that we choose involves simple cluster dynamics at each time step. In terms of the viral model, our focus will be on individual-level transmission via SIR because of its dual relevance to real virus transmission and to the spread of rumors and information in a social system. Here SIR means the viral process susceptible \rightarrow infected \rightarrow recovered, the person-to-person transmission probability at each time step is p and the individual recovery probability at each time step is q , as described in the previous section. Provided that the choice of social dynamics permits similar intrinsic self-amplification and suppression processes by sporadically injecting infected individuals into susceptible groups [see Fig. 1(b) and bottom of Fig. 3], the resulting epidemic profiles from alternative choices of cluster mechanism should exhibit similar characteristics—in particular, multiple resurgences and abnormal decay times (see Figs. 2 and 3). In Sec. VI we extend this SIR focus by presenting quantitative results for other commonly studied viral processes (e.g., SIS).

Our choice of cluster mechanism features the coalescence and fragmentation of groups as described below, and illustrated in Fig. 1(b). There is a huge volume of work in the mathematics, physics and chemistry literature on cluster models within a many-body population of interacting particles [18]. For modern social systems, one is typically interested in mechanisms which mimic the long-range interactions that people can have (either through transport in the case of transmission of viruses, or communications in the case of transmission of a rumor or information). We choose the rate of coalescence of two groups of size n_1 and n_2 , respectively, to be proportional to the combinatorial number of pairwise encounters between individuals, one from each group, i.e., the rate of coalescence is equal to $\nu_{\text{coal}} \cdot (n_1/N) \times (n_2/N)$, where $\nu_{\text{coal}} \leq 1$ is a coalescence probability. Similarly, a given group of n individuals may break up (i.e., completely fragment) with a total rate equal to $\nu_{\text{frag}} \cdot (n/N)$, where $\nu_{\text{frag}} \leq 1$ is a fragmentation probability with $\nu_{\text{frag}} + \nu_{\text{coal}} \leq 1$, reflecting the increasing fragility of large groups (i.e., standard size effect). The implementation of this social dynamics is essentially the same as Ref. [20], with the generalization that the coalescence and fragmentation probabilities are general (i.e., $\nu_{\text{frag}} + \nu_{\text{coal}} \leq 1$ but ν_{frag} is otherwise unrelated to ν_{coal} , in contrast to Ref. [20]). This specific cluster process has real-world relevance for several reasons. First, it embodies the rare but dramatic changes of contact networks that can occur, as mentioned in the introduction. Second, it produces a distribution of group sizes which is power law with exponent 2.5 for $\nu_{\text{coal}} \gg \nu_{\text{frag}}$ when time averaged, as shown in the related model for financial markets [20,21]. This theoretical model is therefore consistent with the observation of Gabaix *et al.* [19] who found that the distribution of transaction sizes follows a power-law with slope near 2.5 for each

of the three major stock exchanges in New York, Paris, and London. Third, this power-law exponent 2.5 is also consistent with the distribution of group sizes inferred for terrorists and insurgent groups based on an analysis of casualty figures [22]. Fourth, the model is structurally robust in that the group dynamic rules can be generalized to different positive power exponents $\alpha \neq 1$, $\beta \neq 1$, $\gamma \neq 1$, with coalescence and fragmentation rates given by $\nu_{\text{coal}} n_1^\alpha \times n_2^\beta$ and $\nu_{\text{frag}} n^\gamma$, respectively, without losing the main qualitative features of the dynamics of the number $I(t)$ of infected individuals.

Individual connectivities within our model may change significantly on the same time scale as the SIR process, thereby mimicking individuals participating in YouTube viewing, financial systems, and schools, who sometimes exhibit rapid moves among peer groups either online or in real space, while simultaneously picking up and spreading rumors or pathogens. A discrete illustration of our model over six time steps is shown in Figs. 1(b) and 1(c). Figure 1(d) contrasts the short-time group structure between individuals with the long-term linkage between them: as time increases without bound, by ergodicity, all individuals will have eventually been part of some common group. While the latter long-time network structure is the one usually emphasized in models of epidemic processes on complex networks, the short-time limited linkage is essential to understand the competition between individual isolation (which tends to stop an epidemic) and group coalescence which amplifies its spreading. In short, this model provides us with a simple framework within which to explore and quantify the interaction of these group dynamical processes and conventional SIR dynamics.

In the numerical implementation of the model, we run the above coalescence-fragmentation dynamics until the time-averaged distribution of group sizes has become stationary. Then, at some instant taken at the origin of time $t=0$, one group is selected, and an arbitrary individual in this group becomes infected, and hence the infection profile unfolds according to the SIR process within each group, with all the groups undergoing at the same time the coalescence-fragmentation dynamics according to the two rates ν_{coal} and ν_{frag} . A typical simulation is shown in Fig. 2, and is compared with the popular approach that models spreading on static networks: (i) an instantaneous network ($T=1$) and (ii) a global network formed by time-aggregating instantaneous contacts over long times ($T \rightarrow \infty$). SIR spreading dynamics on fixed networks obtained at different intermediate T gives curves that lie in the shaded area of Fig. 2. Our model can generate not only this type of dynamics, but also qualitatively new regimes that arise from adjusting the coalescence-fragmentation rates: the large fluctuations, resurgences, and abnormally long decay time which are observed in our model [as illustrated in Fig. 2 (thick curve)] are generated by self-amplification and suppression processes due to the coalescence-fragmentation group dynamics at all group-size scales.

III. THEORETICAL AND EMPIRICAL RESULTS

Figure 3 provides a comparison between two of the empirical profiles that we have collected from each of three

distinct real-world domains, and the theoretical infection profiles $I(t)$ produced by our model. By providing two empirical profiles for each real-world system, our aim is to give confidence that the empirical features observed are not simply the result of some irreproducible external noise. We could generate a number of metrics for comparing the empirical and theoretical profiles (e.g., number of peaks, time interval between peaks, peak-to-trough ratio) as is our intention for future studies when additional data is available—but for now, the message that we wish to convey is a visual one, i.e., that our simple model manages to capture the main qualitative features for each of these three distinct empirical systems.

The sociological example (left column of Fig. 3) shows downloads for two similar YouTube clips [5,6]. Such downloads are typically driven by YouTube users absorbing and spreading opinions as they share information in their social groups [6]. The two downloads appealed to similar age groups, and were measured close together in time, implying that a similar pool of users accessed them both, in line with our model's assumptions. Our model accounts well for the long memory and aftershocklike decay. The top-left panel corresponds to “Gettin’ Enough” from <http://www.youtube.com/watch?v=AiXxMrkekkg>. This video was uploaded to the site on 8 November, 2006 at 13:33:12 GMT. The first record of a download is 9 November, 2006 at 17:21:35 GMT, with a view count of 5708. The last record is 24 May, 2007 at 21:34:30 GMT, with a view count of 257 759. The video's length is 225 s. The middle-left panel shows downloads of music video “Borat” from http://www.youtube.com/watch?v=b1xXERFt_Zg. The video was uploaded to the site on 3 November, 2006 at 11:04:15 GMT. The first record of a download was 7 November, 2006 at 10:35:57 GMT with a view count of 20 745. The last record is 24 May, 2007 at 22:29:25 GMT, with a view count of 254 918. The video's length is 154 s. These two music downloads are similar in terms of appeal, age group, total number of downloads, and lack of any public or global announcement, news, or advertisement, and are hence consistent with spreading through contagion. The bottom-left panel shows our model's output with $\nu_{\text{frag}}=0.05$, $\nu_{\text{coal}}=0.81$, $p=0.001$, and $q=0.001$.

The financial example (middle column of Fig. 3) shows foreign exchange movements as a result of a specific rumor spreading among traders concerning revaluation of the Chinese Yuan currency. This same rumor circulated twice in the space of a few months. The fact that the currency pairs follow a similar dynamical pattern in each case suggests that the same underlying group dynamics developed in line with our model. Note that this financial epidemic is characterized by the largest coalescence rate ν_{coal} and much larger infectivity parameter p among the three examples, reflecting the efficiency of the information cascade among currency traders. The top-center panel corresponds to the CNY (Chinese currency) revaluation rumor as detected from trader chatrooms by HSBC bank (courtesy of S. Williams). Specifically, we show the absolute returns on the time scale of 1 min intervals for the JPY (Japanese currency) exchange rates from 08:22 to 08:53 GMT, on 11 May 2005. The middle-center panel corresponds to the CNY actual revaluation. Ab-

solute returns on the time scale of 1-min intervals are shown for JPY (Japanese currency) exchange rates from 11:03 to 11:34 GMT, on 21 July 2005. Since the CNY was not one of the directly traded currencies, its effects on the JPY- X rates (where X is another currency) are indirect in both cases, suggesting influence through contagion of the rumor or information. There was no public announcement or global news to trigger this activity, which also supports spreading through contagion. The bottom-center panel shows our model output with $\nu_{\text{frag}}=0.05$, $\nu_{\text{coal}}=0.95$, $p=0.009$, and $q=0.002$. Since data are on 1 min scale, but prices can change on 1 s scale, we show an averaged output by providing value at regular equispaced intervals, mimicking 1 min.

The biological example (right column of Fig. 3) shows incidences of a cold among first grade students in two schools in Bogota, Colombia. These data come from an ongoing monitoring experiment carried out by members of our team, in conjunction with the Universidad de Los Andes, Bogota, based on weekly surveys of all students and staff at Colegio Nueva Granada (CNG) and Marymount School. The schools' locations at the top of the Andes guarantee that seasonal temperature variations are minimal. In addition, the student population of each approximates to a closed system due to local issues of security and social segregation. Given the unchanging climatic conditions of this part of Colombia, we argue that the microbes responsible for colds remain present in the environment of children, hence successive bursts can be expected to follow similar dynamics. Within our approach, the school cold dynamics are found to be best described by the lowest fragmentation rate ν_{frag} and highest recovery parameter q , mirroring the more rigid structure of interchildren contacts and the crucial role of multiple recuperations. The bottom-right panel shows our model output with $\nu_{\text{frag}}=0.001$, $\nu_{\text{coal}}=0.5$, $p=0.001$, and $q=0.004$. The model output is smoothed, to mimic fact that data are recorded on the one-week time interval.

The sociological example corresponds to the regime of ν_{coal} values where the group dynamics dominate, hence the strong observed clustering effect in $I(t)$. Large values of ν_{coal} do indeed make sense for social online systems, given the ease and rapidity with which people can now be exposed to new information and rumors through virtual communities. The financial example corresponds to the regime of large transmission probability per time step p , thereby promoting both the spread and survival of the information “virus” and hence leading to persistently noisy (but remarkably reproducible) fluctuations. The biological example seems to lie in between, since it has more peaks as compared with sociological example and larger fluctuations as compared with the financial example. We stress that more complex explanations of each empirical profile in Fig. 3 are undoubtedly possible—and may even be deemed as more realistic by specialists within each field. However, our purpose here is to focus on a minimal description of common dynamical features and to highlight the fact that a common minimal description is indeed possible. Although we have only presented three examples of our model's output, each of which has a quite distinct visual form, it turns out that this subset of three broadly encompasses the full range of $I(t)$ profile behaviors observed across the entire parameter space of our

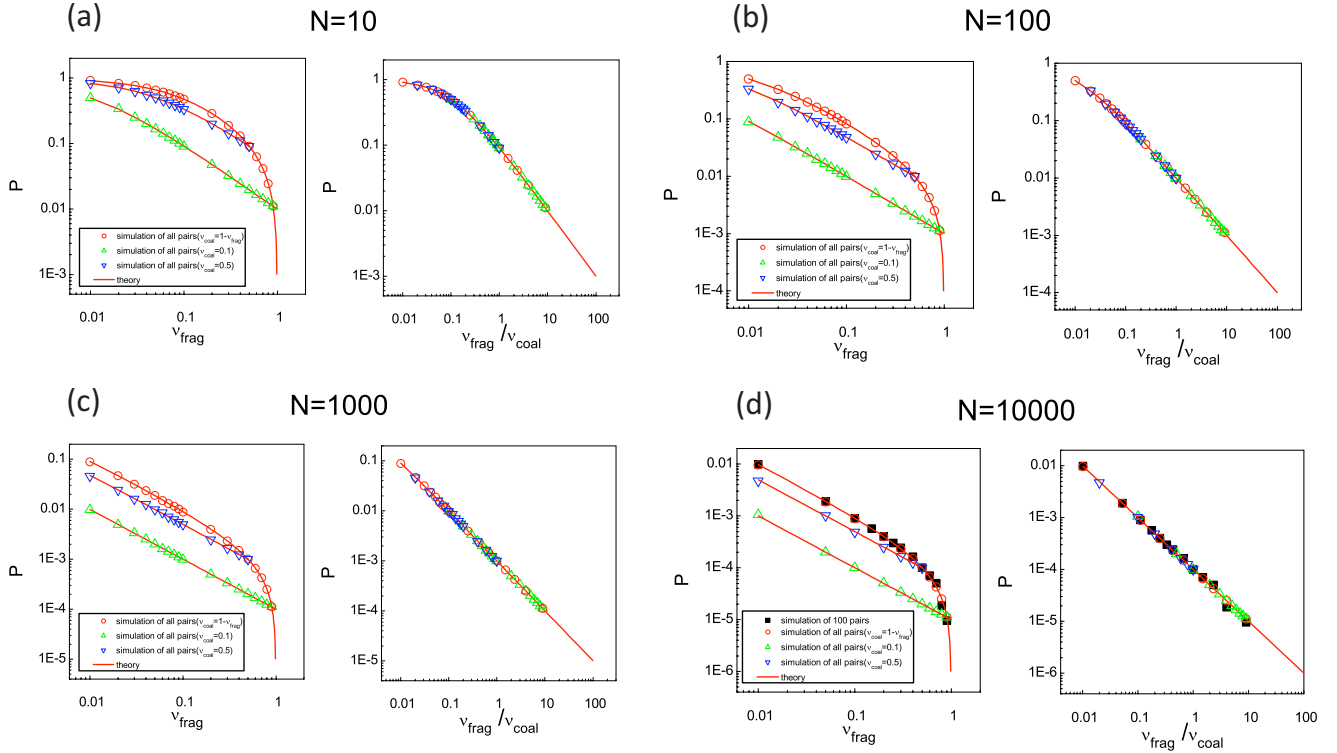


FIG. 4. (Color online) Demonstration of accuracy of Eq. (1) across a range of parameter space. Solid line is theoretical expression from Eq. (1), while discrete points are numerical simulation results. Population size (a) $N=10$, (b) $N=100$, (c) $N=1000$, and (d) $N=10\,000$. Left panel for each N value: P value obtained by tracking all pairs over time for the illustrative case ($\nu_{\text{coal}} + \nu_{\text{frag}} = 1$), and also for specific values $\nu_{\text{coal}} = 0.1$ and 0.5 . Left panel of (d) additionally shows result of tracking just 100 pairs over time, demonstrating that the same results are obtained as long as the time window is sufficiently long. Right panel for each N value: P as a function of $\nu_{\text{frag}} / \nu_{\text{coal}}$ on a log-log scale. Data corresponding to different systems fall onto the same curve as predicted by Eq. (1).

model. One might speculate whether other empirical examples chosen from social, financial, and biological domains, might also fall crudely into one of these three classes of infection profile behavior shown in Fig. 3. A casual observation of similar types of empirical data available on the web suggests that this might indeed be the case [6,24].

IV. APPROXIMATE ANALYTIC ANALYSIS

A. Limiting case relationship with mass-action epidemiological theory

A full analytic description of the $I(t)$ profiles generated by our model represents a fascinating open challenge for the community. However some important features can be captured straight away by suitably generalizing existing epidemiological machinery. A key quantity is the probability $\eta_{\text{SI}}(t)$ that a particular link instantaneously exists *and* that it connects a susceptible and an infected. Thus, out of a potential totality of $N(N-1)/2$ links among N individuals, only $\eta_{\text{SI}}(t)N(N-1)/2$ are typically present. This provides an accurate equation for the number of susceptibles $S(t)$ in a given epidemic sequence: $\dot{S}(t) = -p\eta_{\text{SI}}(t)N(N-1)/2$, with p is the infectivity parameter quantifying the probability that a particular S is infected by a particular I to which it is linked. We rewrite this in the conventional mass-action form $\dot{S}(t) = -pP_{\text{SI}}(t)S(t)I(t)$, where $P_{\text{SI}}(t)$ is equivalent to $\eta_{\text{SI}}(t)N(N-1)/[2S(t)I(t)]$ and hence now incorporates the complex dynamics which are so hard to capture analytically. We now approximate $P_{\text{SI}}(t)$ by a constant term P , which is the time-averaged probability that any two arbitrarily chosen nodes belong to the same cluster independent of SI -infection status. This approximation throws out the dynamical details of $I(t)$ but can provide useful insights, as shown below on the non-spreading to spreading transition, provided that several coalescence-fragmentation processes occur over the time scale of the entire outbreak. In order to develop a more detailed analytic analysis, we start with the identification of P as the average value of $P_{i,j}$, where $P_{i,j}$ means the probability that specific nodes i and j are connected (i.e., i and j are in the same cluster). Our numerical simulations enable us to track individual pairs and hence deduce numerical values for P as a function of ν_{coal} , ν_{frag} , and N .

Figure 4 presents P values taken from the numerical simulation, which suggest that P has a remarkably simple functional form. Results are shown for populations of size $N=10$ [Fig. 4(a)], $N=100$ [Fig. 4(b)], $N=1000$ [Fig. 4(c)], and $N=10\,000$ [Fig. 4(d)], and for different sets of parameters ν_{coal} and ν_{frag} . There are several ways that one can obtain the quantity P numerically. One could follow a certain pair of nodes over a very long simulation run of the model, counting how many time steps these two nodes happen to be in the same cluster. Alternatively, to reduce run times, one may follow a certain number of pairs (e.g., 50 or 100) over a

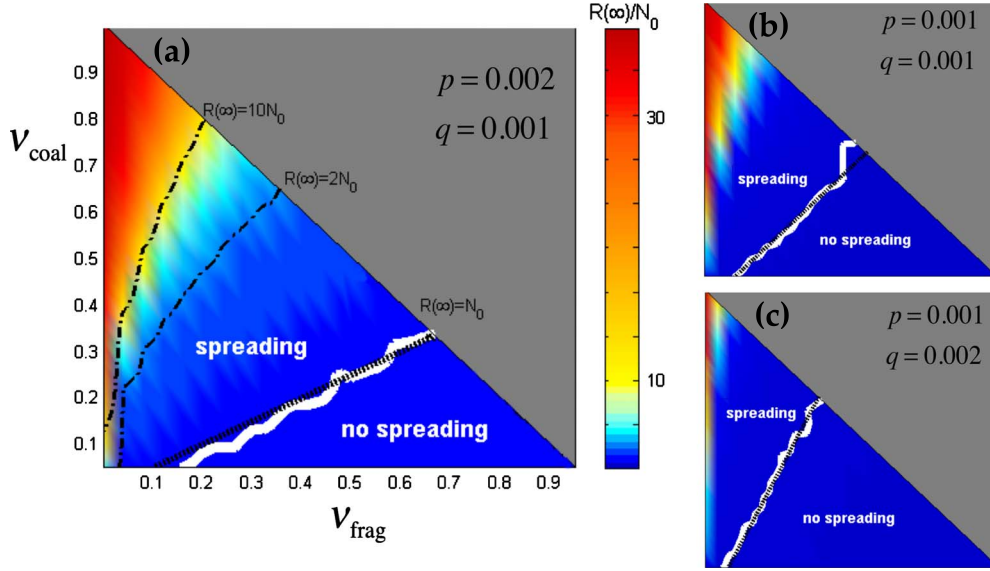


FIG. 5. (Color online) Phase diagrams show theoretically obtained transition (i.e., $\frac{p\nu_{\text{coal}}}{q\nu_{\text{frag}}} = 1$, black dashed line) and the numerical result (white solid line) separating regimes of spreading [i.e., overall number of infecteds exceeds initial group size, hence $R(\infty) > N_0$] and no spreading [i.e., $R(\infty) < N_0$]. Population reacts to news of the initial infection at $t=0$ by changing its dynamical grouping from $\nu_{\text{frag}}=0.001$ and $\nu_{\text{coal}}=0.99$, to the new values shown on the axes. Shading shows the population (in units of N_0) who become infected, and hence recovered, over the lifetime of the outbreak. Solid triangular shaded region is unphysical since $\nu_{\text{frag}} + \nu_{\text{coal}} > 1$.

particular time window. As confirmed by the left-hand panel of Fig. 4(d), the results do not depend on the precise method used. The numerical results in Fig. 4 suggest that the variation in P can be well described by the following empirical relation:

$$P = \frac{\nu_{\text{coal}}}{\nu_{\text{coal}} + N\nu_{\text{frag}}} = \frac{1}{1 + N\frac{\nu_{\text{frag}}}{\nu_{\text{coal}}}}. \quad (1)$$

This expression contains an explicit dependence on N , the number of nodes in the system, and a dependence on the ratio $\nu_{\text{frag}}/\nu_{\text{coal}}$. For each N value in Fig. 4, the right-hand panel shows that different simulations with different parameters ($\nu_{\text{coal}}, \nu_{\text{frag}}$) yield dependences of P as a function of $\nu_{\text{frag}}/\nu_{\text{coal}}$ which all collapse on the same curve. For $N\nu_{\text{frag}} \gg \nu_{\text{coal}}$, Eq. (1) reduces to the approximate form

$$P = \frac{\nu_{\text{coal}}}{N\nu_{\text{frag}}}. \quad (2)$$

B. Analytic derivation of P using master equation

Having demonstrated the quantitative accuracy of Eq. (1) using quantitative results from the model simulation, we now turn to the task of trying to understand this result analytically. Starting with the master equation approach, the dynamics of $P_{i,j}$ follows

$$\begin{aligned} \frac{dP_{i,j}}{dt} = & -P_{i,j} \frac{1}{N} \sum_{k \in \{..i\}} P_{k,i} \nu_{\text{frag}} + (1 - P_{i,j}) \\ & \times \frac{1}{N} \sum_{m \in \{..i\}} P_{m,i} \frac{1}{N} \sum_{n \notin \{..i\}} P_{n,j} \nu_{\text{coal}}. \end{aligned} \quad (3)$$

As indicated, the sums are restricted to either the nodes within the cluster containing node i or to the nodes outside that cluster. We note that the first term on the right-hand side can alternatively be written in a completely symmetric way in terms of i and j , simply by splitting the term into two equal pieces (one in i and one in j) and adding a factor of one half to avoid double counting. Two particular situations will significantly affect the value of $P_{i,j}$: one situation is where the nodes i and j are together but are going to breakup at the next time step. The second situation is where the node i and j are not currently together but are going to join together at the next timestep. The two terms on the right-hand side of Eq. (3) correspond to these two cases. The first term on the right-hand side of Eq. (3) describes the case where nodes i and j are together ($P_{i,j}$) and then one node k is picked ($\frac{1}{N}$) which is in the same cluster as i and j ($P_{k,i}$) and so the cluster fragments (ν_{frag}). The second term of Eq. (3) describes the case where nodes i and j are not together ($1 - P_{i,j}$), and then one node m is picked ($\frac{1}{N}$) which is in the same cluster as i ($P_{m,i}$), as well as one node n being picked ($\frac{1}{N}$) in the same cluster as j ($P_{n,j}$). They then coalesce (ν_{coal}). We stress that the third summation $\sum_{n \notin \{..i\}}$ sums over all the nodes outside the cluster containing node i , and hence $\sum_{n \notin \{..i\}} P_{n,j} = 1$. In the steady state, we can write $P = P_{i,j}$ for all i and j . The remaining two summations over nodes within the cluster containing node i , then become equal to the average cluster size multi-

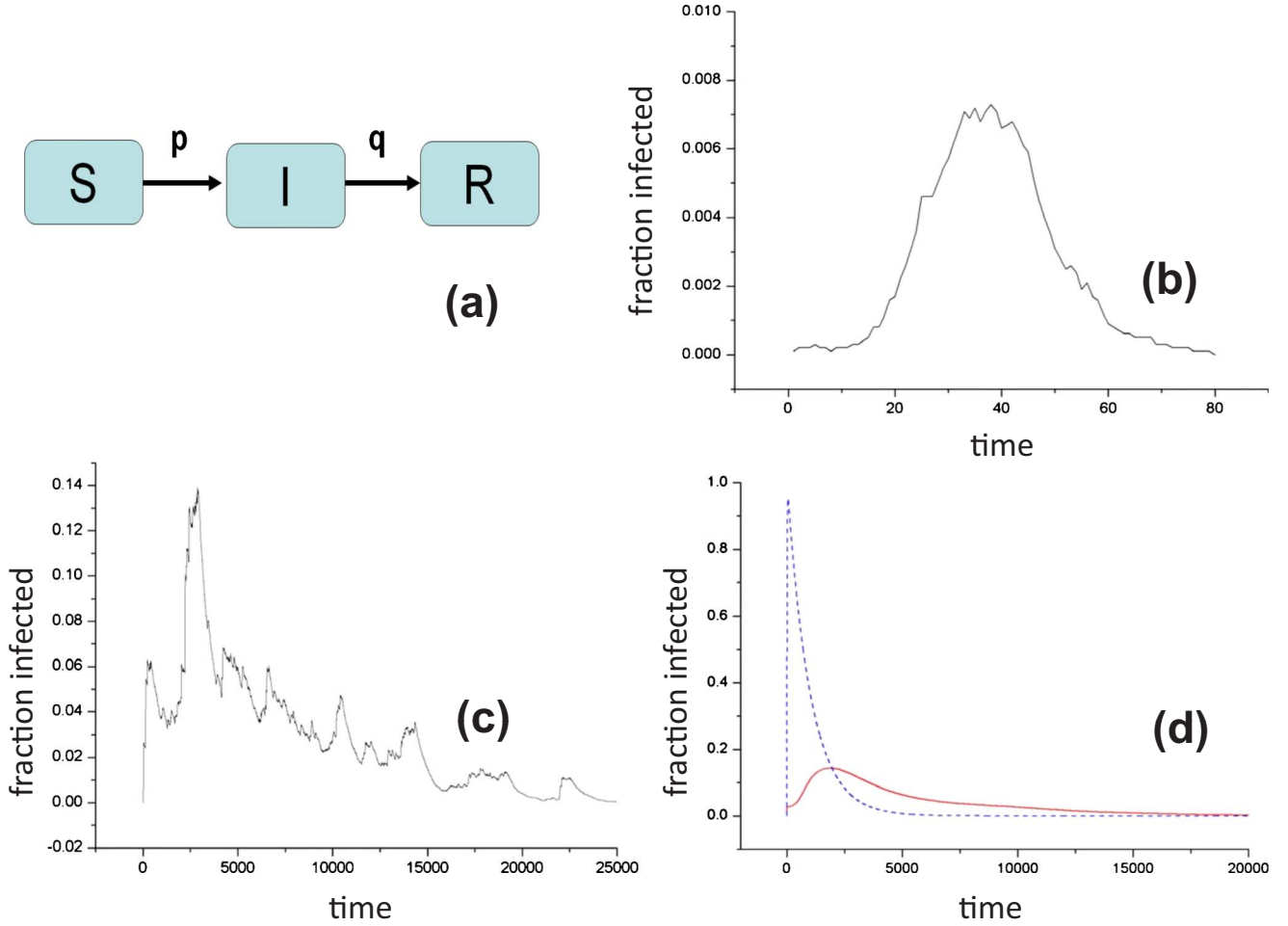


FIG. 6. (Color online) SIR process in presence of the coalescence-fragmentation group dynamics. (a) Schematic SIR process. (b) Typical individual simulation run showing $I(t)$ for $N=10\,000$, $\nu_{\text{frag}}=0.001$, $\nu_{\text{coal}}=0.99$, $p=0.001$, and $q=0.1$. (c) Typical individual simulation run showing $I(t)$ for $N=10\,000$, $\nu_{\text{frag}}=0.01$, $\nu_{\text{coal}}=0.9$, $p=0.001$, and $q=0.001$. (d) Comparison between run-averaged $I(t)$ (solid curve, red) using the same parameters as (c), and $I(t)$ for a weighted network (blue dotted curve) in which all nodes are connected with strength P .

plied by P . Setting the left-hand side of Eq. (3) equal to zero and solving for P yields

$$P = \frac{\nu_{\text{coal}}}{\nu_{\text{coal}} + N\nu_{\text{frag}}} = \frac{1}{1 + N\frac{\nu_{\text{frag}}}{\nu_{\text{coal}}}},$$

which is exactly Eq. (1).

C. Analytic derivation of P using coupled cluster equations

The limiting case Eq. (2) can also be obtained in the limit $N\nu_{\text{frag}} \gg \nu_{\text{coal}}$, by considering the master equation for the number n_s of clusters with size s in the model:

$$\begin{aligned} \frac{\partial n_s}{\partial t} = & -\frac{\nu_{\text{frag}} s n_s}{N} + \frac{\nu_{\text{coal}}}{N^2} \sum_{s'=1}^{s-1} s' n_{s'} (s-s') n_{s-s'} \\ & - \frac{2\nu_{\text{coal}} s n_s}{N^2} \sum_{s'=1}^{\infty} s' n_{s'} \end{aligned} \quad (4)$$

for $s \geq 2$, with a similar but truncated form for $s=1$,

$$\frac{\partial n_1}{\partial t} = \frac{\nu_{\text{frag}}}{N} \sum_{s'=2}^{\infty} (s')^2 n_{s'} - \frac{2\nu_{\text{coal}} n_1}{N^2} \sum_{s'=1}^{\infty} s' n_{s'}. \quad (5)$$

For a steady-state cluster distribution, we have

$$s n_s = \frac{\nu_{\text{coal}}}{2\nu_{\text{coal}} + \nu_{\text{frag}}} \frac{1}{N} \sum_{s'=1}^{s-1} s' n_{s'} (s-s') n_{s-s'} \quad (6)$$

for $s \geq 2$, while for $s=1$ we have

$$n_1 = \frac{\nu_{\text{frag}}}{2\nu_{\text{coal}}} \sum_{s'=2}^{\infty} (s')^2 n_{s'}. \quad (7)$$

Therefore on average, we obtain

$$P = \sum_{s=2}^{\infty} \frac{s n_s}{N} \frac{s-1}{N} = \frac{1}{N^2} \sum_{s=2}^{\infty} (s^2 n_s - s n_s) = \frac{1}{N^2} \frac{2\nu_{\text{coal}}}{\nu_{\text{frag}}} n_1 - \frac{N-n_1}{N^2}, \quad (8)$$

where the only unknown quantity is n_1 . We now define a generating function,

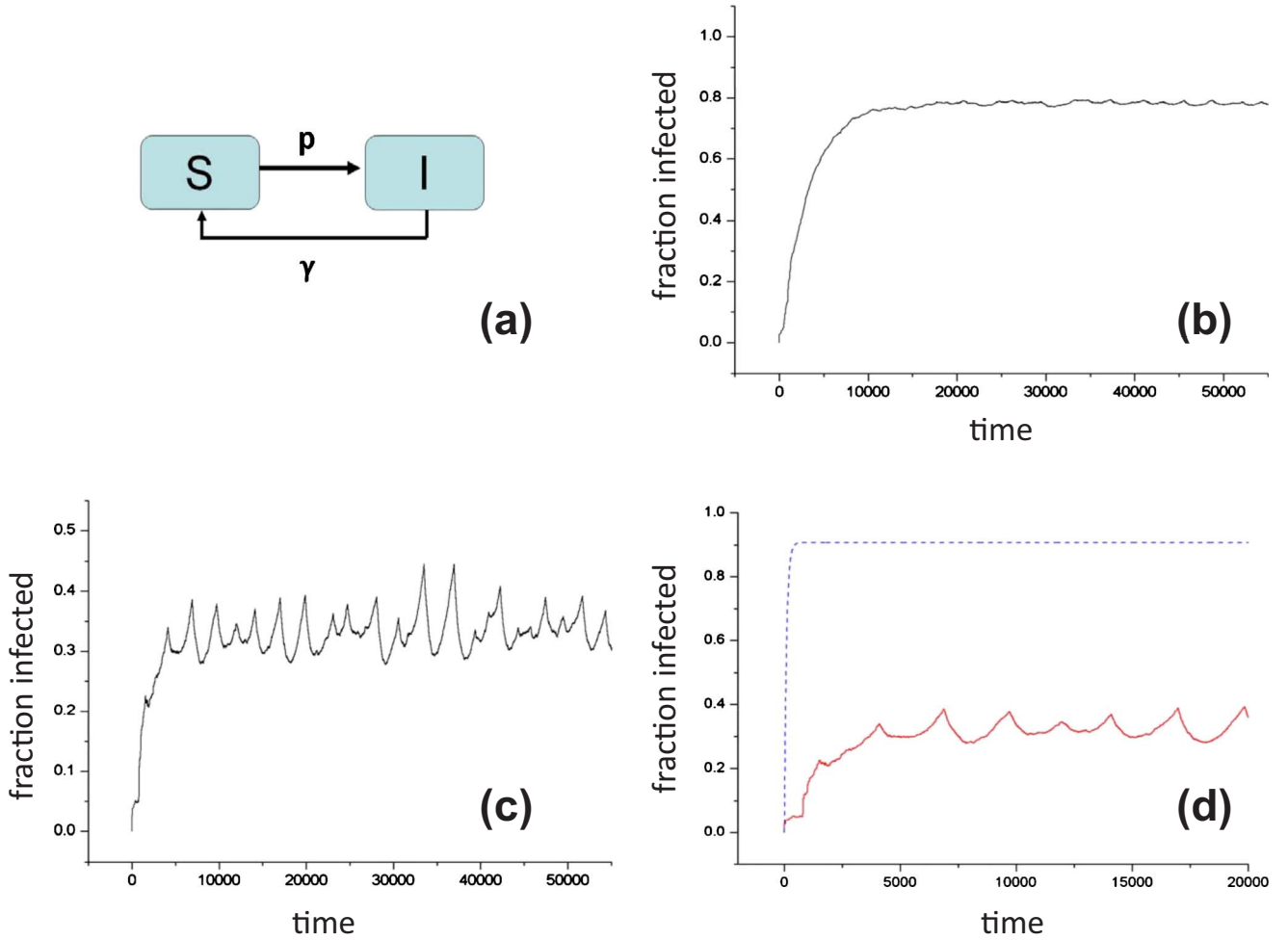


FIG. 7. (Color online) SIS process in presence of the coalescence-fragmentation group dynamics. (a) Schematic SIS process. (b) Typical individual simulation run showing $I(t)$ for $N=10\,000$, $\nu_{\text{frag}}=0.01$, $\nu_{\text{coal}}=0.99$, $p=0.01$, and $\gamma=0.0001$. (c) Typical individual simulation run showing $I(t)$ for $N=10\,000$, $\nu_{\text{frag}}=0.001$, $\nu_{\text{coal}}=0.99$, $p=0.01$, and $\gamma=0.001$. (d) Comparison between $I(t)$ (solid curve, red) using the same parameters as (c), and $I(t)$ for a weighted network (blue dotted curve) in which all nodes are connected with strength P .

$$G[y] = \sum_{k=0}^{\infty} kn_k y^k = n_1 y + \sum_{k=2}^{\infty} kn_k y^k = n_1 y + g[y]. \quad (9)$$

Taking Eq. (6) multiplied by y^s and then summing from $s=2$ to ∞ yields

$$g[y] = \frac{\nu_{\text{coal}}}{2\nu_{\text{coal}} + \nu_{\text{frag}} N} G[y]^2, \quad (10)$$

i.e.,

$$g[y]^2 - \left(\frac{2\nu_{\text{coal}} + \nu_{\text{frag}} N}{\nu_{\text{coal}}} - 2n_1 y \right) g[y] + n_1^2 y^2 = 0, \quad (11)$$

where $g[y] = \sum_{s=2}^{\infty} s n_s y^s$ and $g[1] = N - n_1$. Solving this quadratic equation Eq. (11) gives

$$n_1 = \frac{\nu_{\text{frag}} + \nu_{\text{coal}}}{\nu_{\text{frag}} + 2\nu_{\text{coal}}} N. \quad (12)$$

Substituting into Eq. (8), we obtain Eq. (2).

V. DYNAMICAL CONTROL OF OUTBREAKS

We now use our numerical model and the approximate analytic analysis of Sec. IV, in order to address the following highly topical question: will there be epidemic spreading in a population in which it is publically known that N_0 persons have been infected with a given pathogen or rumor, but where the precise identity of infected persons cannot be disclosed? At $t=0$, $N_0 \ll N$ individuals of the instantaneously largest group are infected and news of an infection is announced without disclosing the infected's identities. The population reacts by adjusting its group dynamics, i.e., it adopts a new ν_{coal} and ν_{frag} . Although many further features could be added to mimic the population's subsequent adjustment to knowledge of an outbreak, we focus here on a simple case in order to better understand the effect of the initial reaction.

Numerical results are presented in Fig. 5, together with analytic curves for the transition threshold, as a function of the new ν_{coal} and ν_{frag} . Our analytic analysis exploits the generalized SIR equations developed in Sec. IV, and builds upon the theoretical framework discussed in detail in Ref.

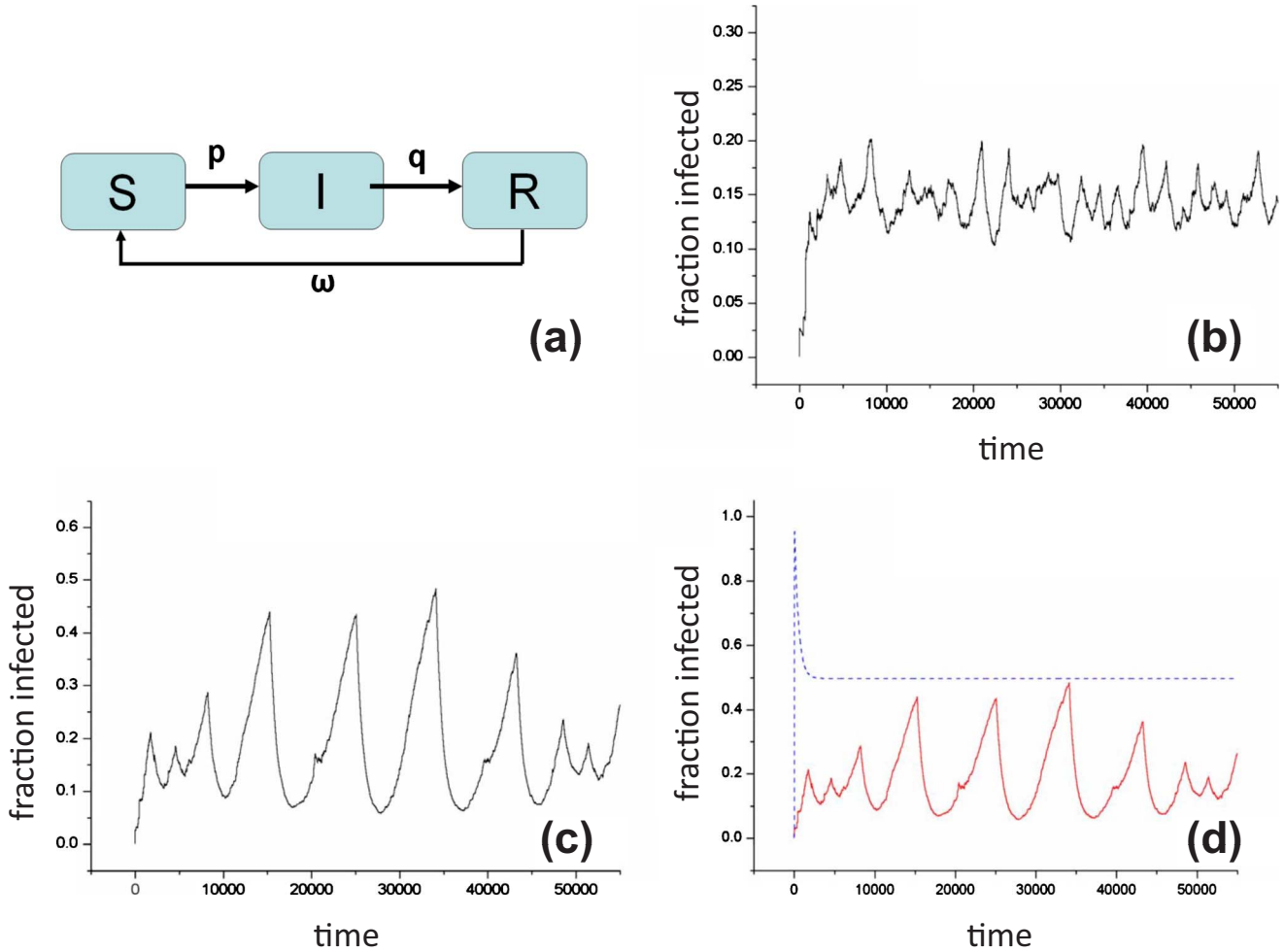


FIG. 8. (Color online) SIRS process in presence of the coalescence-fragmentation group dynamics. (a) Schematic SIR process. (b) Typical individual simulation run showing $I(t)$ for $N=10\,000$, $\nu_{\text{frag}}=0.01$, $\nu_{\text{coal}}=0.99$, $p=0.01$, $q=0.001$, and $\omega=0.001$. (c) Typical individual simulation run showing $I(t)$ for $N=10\,000$, $\nu_{\text{frag}}=0.001$, $\nu_{\text{coal}}=0.99$, $p=0.01$, $q=0.001$, and $\omega=0.001$. (d) Comparison between $I(t)$ (solid curve, red) using the same parameters as (c), and $I(t)$ for a weighted network (dotted curve, blue) in which all nodes are connected with strength P .

[12]. The number of susceptibles in the long-time limit $S(\infty)$ with $N \gg 1$ is then given by the solution \bar{z} to the following generalized form, $z = \exp[-\kappa(1-z)]$ where $z \equiv S(\infty)/N$ and $\kappa \equiv p\nu_{\text{coal}}/q\nu_{\text{frag}}$ where κ plays the role of the basic reproductive rate. For $\kappa \leq 1$, the only solution is $\bar{z} = 1$, corresponding to a vanishingly small fraction of infected individuals [i.e., total number of infected $R(\infty)$ does not exceed $N_0 \ll N$]. This solution bifurcates at $\kappa = 1$ into the following stable solution $\bar{z} = -(1/\kappa)W(-\kappa e^{-\kappa})$ valid for $\kappa > 1$, where $W(z)$ is the Lambert function. For $\kappa > 1.5$, \bar{z} is very well-approximated by $\bar{z} \approx e^{-\kappa}/\kappa$. This shows a rather abrupt transition from non-spreading epidemics for $\kappa < 1$ to global infection of a finite fraction of the population for $\kappa > 1$. The form of the epidemic control parameter $\kappa \equiv p\nu_{\text{coal}}/q\nu_{\text{frag}}$ exemplifies that infectivity and coalescence play together against recovery and fragmentation in controlling the propagation of the epidemics: Infectivity and coalescence promote the infection propagation, while recovery and fragmentation hinders its spread.

Not only is our theory for the spreading threshold (dashed black line in Fig. 5) in good agreement with the numerical results (white solid line), its simple analytic form suggests an

epidemic control scheme based on manipulation of the group coalescence and fragmentation time scales (i.e., ν_{coal}^{-1} and ν_{frag}^{-1}). An imminent epidemic can be *suppressed* [i.e., $R(\infty) < N_0$] by increasing the time scale for group coalescence with respect to the time scale for group fragmentation (i.e., decrease ν_{coal} with respect to ν_{frag}), but it will get *amplified* if we decrease the coalescence time scale with respect to the fragmentation time scale (i.e., increase ν_{coal} with respect to ν_{frag}). Not only would such modest intervention allow the overall system to continue functioning, it does *not* require knowledge of the infected's identities. There is also no assumption that the N_0 members of the group which carries the initial infected case at $t=0$, remain in that group. In the school setting, schedules could be adjusted to slow down or speed up classroom use and recess, without the need for disruptive school closures [3] or the need to test, label, or isolate infected children. In particular, the coalescence rate in a school could be reduced by simply staggering the lunch-times for separate classes, as opposed to isolating them entirely. Having individual classes in the cafeteria at different times does not count as a coalescence event, while a com-

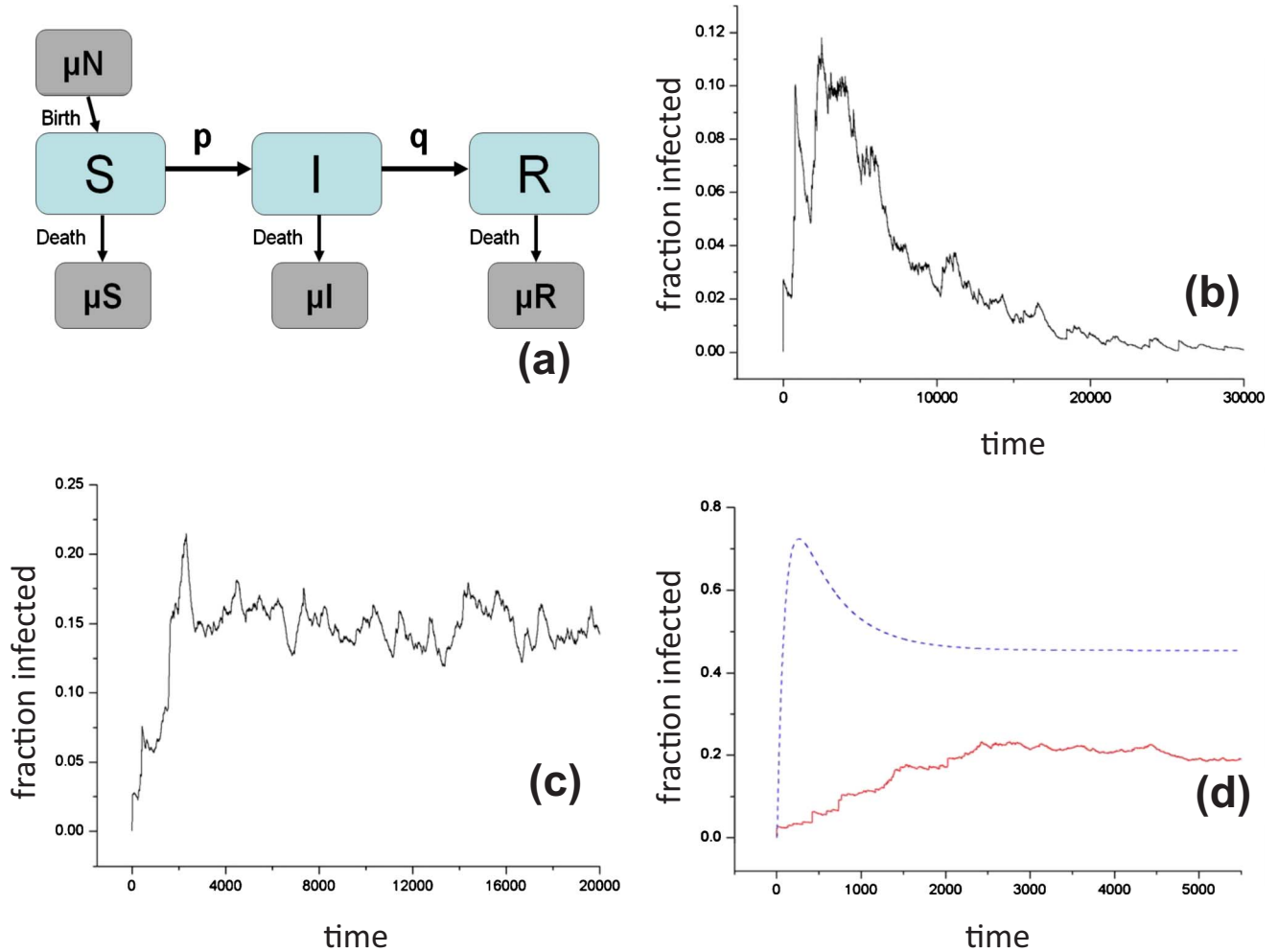


FIG. 9. (Color online) SIRD process (i.e., SIR with demography) in presence of the coalescence-fragmentation group dynamics. (a) Schematic SIR process. (b) Typical individual simulation run showing $I(t)$ for $N=10\,000$, $\nu_{\text{frag}}=0.01$, $\nu_{\text{coal}}=0.99$, $p=0.01$, $q=0.001$ and $\mu=0.000\,001$. (c) Typical individual simulation run showing $I(t)$ for $N=10\,000$, $\nu_{\text{frag}}=0.01$, $\nu_{\text{coal}}=0.99$, $p=0.01$, $q=0.001$, and $\mu=0.001$. (d) Comparison between $I(t)$ (solid curve, red) using the same parameters as (b) but with $\mu=0.001$, and $I(t)$ for a weighted network (blue dotted curve) in which all nodes are connected with strength P .

mon lunchtime period would. Hence the coalescence rate can be reduced without removing any of the daily routine activity. In financial markets, if one wanted to prevent highly noisy fluctuations of the type observed in Fig. 3, similar control might be achieved by basing the joining and leaving rules of the online chat rooms frequented by financial traders, on present occupancy. In viral marketing, the attractiveness of the message or product quantified by the infectivity p can be completely subjugated by suitable management of the group dynamics (ν_{coal} versus ν_{frag}), as firms using e-commerce and e-advertisement are now realizing [23]. These findings are potentially applicable to many other scenarios, given that many real-world activity and infection curves resemble those in Fig. 2.

VI. RESULTS FOR GENERAL INFECTION MODELS

Having focused exclusively on the SIR viral process, we now compare the infection profiles generated using other commonly studied viral processes. To ease comparison, the

population maintains the *same* coalescence-fragmentation group dynamics as featured throughout this paper. We find that a similarly large range of $I(t)$ profiles arise for these other viral processes as for SIR, which is understandable given that they are all being driven by the same background group dynamics. In addition to p and q , some of the viral processes will use μ which is a birth and death probability rate, γ which is a probability rate of transition from I to S , and ω is a probability rate of transition from R to S .

As suggested in the earlier parts of this paper, we might expect the numerical simulations to exhibit three main classes of behavior for each type of viral process: (1) group dynamics is much slower than epidemic spreading, hence the virus tends to exist only within the initial group; (2) group dynamics is comparable with the epidemic spreading, hence grouping plays a significant role in suppressing or amplifying the spreading leading to generic spiky behavior in the infection profile $I(t)$; (3) group dynamics is much faster than epidemic spreading, in which case analytic theory can be developed as discussed earlier in Sec. IV for SIR. Figure 6 summarizes some typical results from the SIR process in the

presence of group dynamics, as discussed throughout this paper. As in Fig. 3, a broad range of $I(t)$ profiles can be obtained—in particular those with large resurgences and a long-tailed decay—simply by varying ν_{coal} , ν_{frag} , p , and q . Neither individual nor time-averaged runs can be explained by considering the SIR process on a static weighted network. This is because any static network model neglects the dynamically changing nature of the transmission pathways, i.e., the dynamically changing contact structure.

Figure 7 presents the SIS viral process which is appropriate for diseases without immunity. Recovery from infection is followed by an instant return to the susceptible pool. The slow growth and low stable state (endemic equilibrium) are both due to suppression by the group dynamics, which only allows a part of the population to come in contact with infecteds, while others are isolated in different groups. Before an infected node can contact the whole population and infect them, it may recover and become susceptible again. Figures 7(b) and 7(c) show how the restoration rate γ , combined with ν_{frag} and ν_{coal} , affect the stability of $I(t)$ after reaching the endemic equilibrium. Large γ values yield large jumps, and vice versa, because it leads to quickly replenishment of the pool of susceptibles. Figure 8 presents the SIRS viral process which is appropriate for diseases in which an infected has a recovery time and then returns to susceptible status. It appears similar to SIS, but produces bigger fluctuations than SIS since there is the possibility that infecteds maintain an inert state (R) for a finite time, which hence allows $I(t)$ to become very small. The net effect is that the $I(t)$ peak-trough ratio is enhanced as compared to SIS.

Figure 9 presents the SIRD viral process which corresponds to the addition of demography (i.e., births and deaths) to SIR. It assumes that there is a natural mortality μ (i.e., each individual has a lifespan $1/\mu$). In order to keep the total population constant $S+I+R=N$, μ also represents the birth rate of the population. Figure 9(b) shows that when the birth-death processes are much slower than infection and recovery processes, the infection profile $I(t)$ is essentially the same as SIR model including group dynamics. The fact that the endemic equilibrium is not stable can be solved by increasing μ . However we stress that as in all other cases, the resultant $I(t)$ profile is different from the corresponding result for a static weighted network [Fig. 9(d)].

VII. SUMMARY AND OUTLOOK

We have presented and analyzed a simple model of contagion within a population featuring dynamically evolving connectivity, allowing group-level dynamics and the individual-level transmission process to coexist on similar time scales. In spite of the simplicity of our model, we find that the profiles produced bear a striking resemblance to a wide variety of real-world examples from social, financial, and biological domains. The common features of multiple resurgent peaks and abnormal decay times are observed both theoretically and empirically. To demonstrate further the generic nature of the empirical profiles that we show in Fig. 3, and hence the relevance of our theoretical model, we refer interested readers to examine the explicit YouTube profiles in Ref. [6], and the wider range of examples in Ref. [24]. In terms of further justifying the underlying group dynamics that we imposed, we stress that the recent Ref. [22] shows explicitly that these coalescence-fragmentation group dynamics are consistent with that observed in insurgencies. Adding in the feature of transmission, as we do in the present paper, elevates this particular real-world application to the hotly debated issue of understanding how information and know-how about improvised explosive devices (IEDs)—in particular innovations in design—spreads through an insurgency. This latter topic is a very important practical one given the recent insurgent preference for IED use in the current wars in Iraq and Afghanistan.

Although it is of course possible that such empirically observed $I(t)$ profiles can be generated by other more sophisticated models—e.g., more detailed social dynamic mechanisms, the introduction of spatial heterogeneity, or more elaborate generalizations of the SIR transmission process—we find it intriguing that our simple analysis suffices. We hope that these findings stimulate future work on the potential effects of different social group dynamics (see, for example, Palla *et al.* [17]) and on detailed analytic descriptions of the resulting infection profiles.

ACKNOWLEDGMENT

One of us (P.M.H) acknowledges the support from the Research Grants Council of the Hong Kong SAR Government under Grant No. CUHK-401109.

-
- [1] F. E. Harmon, Emergency Order by U.S. Securities and Exchange Commission: *False Rumors can Lead to a Loss of Confidence in our Markets*, Release Number 58166, July 15, 2008.
 - [2] D. G. McNeil, *Containing Flu is not Feasible, Specialists Say*, New York Times, Front Page, Thursday, April 30, 2009.
 - [3] Report by The American Academy of Pediatrics (AAP), *Pandemic Influenza: Warning Children At-Risk* (2007).
 - [4] S. Lyall, *Susan Boyle, Unlikely Singer is YouTube Sensation*, New York Times, Front Page, Friday, April 17, 2009.
 - [5] D. Sornette, F. Deschâtres, T. Gilbert, and Y. Ageon, *Phys. Rev. Lett.* **93**, 228701 (2004).
 - [6] R. Crane and D. Sornette, *Proc. Natl. Acad. Sci. U.S.A.* **105**, 15649 (2008).
 - [7] M. J. Keeling and P. Rohani, *Modeling Infectious Diseases in Humans and Animals* (Princeton University Press, Princeton, NJ, 2007).
 - [8] R. M. May and A. L. Lloyd, *Phys. Rev. E* **64**, 066112 (2001).
 - [9] F. Ball, D. Mollison, and G. Scalia-Tomba, *Ann. Appl. Probab.* **7**, 46 (1997).
 - [10] J. Shao, S. Havlin, and H. E. Stanley, *Phys. Rev. Lett.* **103**, 018701 (2009).
 - [11] J. S. Koopman, in *Biological Networks*, edited by F. Kepes

- (World Scientific, London, 2007).
- [12] J. D. Murray, *Mathematical Biology: I. An Introduction*, 3rd ed. (Springer, New York, 2007), Chap. 10.
- [13] V. Colizza and A. Vespignani, *Phys. Rev. Lett.* **99**, 148701 (2007).
- [14] D. J. Watts, R. Muhamad, D. C. Medina, and P. S. Dodds, *Proc. Natl. Acad. Sci. U.S.A.* **102**, 11157 (2005); P. S. Dodds and D. J. Watts, *Phys. Rev. Lett.* **92**, 218701 (2004).
- [15] T. Gross, C. Dommar, and B. Blasius, *Phys. Rev. Lett.* **96**, 208701 (2006).
- [16] L. B. Shaw and I. B. Schwartz, *Phys. Rev. E* **77**, 066101 (2008).
- [17] G. Palla, A. L. Barabasi, and T. Vicsek, *Nature (London)* **446**, 664 (2007).
- [18] M. Smoluchowski, *Phys. Z.* **17**, 557 (1916); J. A. D. Wattis, *Physica D* **222**, 1 (2006).
- [19] X. Gabaix, P. Gopakrishnan, V. Plerou, and H. E. Stanley, *Q. J. Econ.* **121**, 461 (2006).
- [20] V. M. Eguíluz and M. G. Zimmermann, *Phys. Rev. Lett.* **85**, 5659 (2000).
- [21] N. F. Johnson, P. Jefferies, and P. M. Hui, *Financial Market Complexity* (Oxford University Press, New York, 2003).
- [22] J. C. Bohorquez, S. Gourley, A. R. Dixon, M. Spagat, and N. F. Johnson, *Nature (London)* **462**, 911 (2009); N. F. Johnson, in *Managing Complexity: Insights, Concepts, Applications*, edited by D. Helbing (Springer, Berlin, 2008), p. 303.
- [23] R. Colbaugh and K. Glass, e-print [arXiv:0912.5242](https://arxiv.org/abs/0912.5242); *Social Marketing* at <http://knowledge.wharton.upenn.edu/article.cfm?articleid=1864>; J. Leskovec, M. McGlohon, C. Faloutsos, N. Glance, and M. Hurst, e-print [arXiv:0704.2803v1](https://arxiv.org/abs/0704.2803v1); R. Dye, *Harvard Bus. Rev.*, Nov-Dec issue, pg. 139 (2000).
- [24] Additional candidate “infection” profiles where the contagion activity level $I(t)$ is measured as web hits, downloads etc., and where $I(t) \sim 0$ before the initial event, as expected for an outbreaklike contagion phenomenon: (i) swine flu at the level of a county, state, or country, following initial cases—for example, Florida, U.S. at http://www.doh.state.fl.us/Disease_ctrl/epi/swineflu/Reports/reports.htm; (ii) Code-Red outbreak of Internet worm, see D. Moore, C. Shannon, and K. Claffy at <http://www.icir.org/vern/imw-2002/>; (iii) SARS virus, see p. 18 at <http://www.who.int/csr/sars/WHOconsensus.pdf>; (iv) website hits for movie *Brokeback Mountain* following death of actor Heath Ledger. Prior to his death, the web traffic had been essentially zero [i.e., $I(t) \sim 0$ as required] for an extended period. See <http://www.alexa.com/> for *Brokeback Mountain*; (v) website hits for a new album by band Radiohead in October 2007. See <http://www.alexa.com/> for in rainbows; (vi) outbreak of number of improvised explosive devices (IEDs) in Afghanistan following their first reported use. See <http://www.icasualties.org/OEF/Index.aspx>